The Changing Brain in Healthy Aging: a multi-MRI machine and multicenter surface-based morphometry study

P. Donnelly Kehoe[a, b], G. Pascariello[a], M. Quaglino [c], J. Nagel [b, d] and J.C. Gómez[a]
[a]Laboratory for System Dynamics and Signal Processing, Universidad Nacional de Rosario, CIFASIS-CONICET, Rosario, Argentina.
[b] Maestría en Neurociencias y Neurotecnologías, Facultad de Ciencias Médicas, Universidad Nacional de Rosario, Argentina.
[c] Facultad de Ciencias Económicas y Estadística, Universidad Nacional de Rosario, Argentina.
[d] Neurorradiology Service, Instituto Gamma, Rosario, Argentina.

ABSTRACT

Clinical practice on magnetic resonance imaging of the brain has been historically based on a comparative analysis using a well-trained eye to see whether different features corresponded to a healthy pattern or not. Several studies have described that healthy aging is associated with loss in tissue volume and expansion of cerebrospinal fluid cavities, making this healthy pattern a dynamical and complex model. For these reasons we propose that structural neurorradiology should be assisted by a quantitative and statistical model that can give meaning to a patient's brain morphometric measurements, giving additional information to the clinician about possible deviations from health. With this aim we obtained normative brain morphometric values by applying an automated voxel and surface-based processing pipeline using the well-known software package FreeSurfer. Employing the publicly available IXI Dataset created by Imperial College London we obtained 135 metrics of the aging process from 538 participant between 20 and 86 years old. In concordance with previous studies we found evidence of change in almost all analyzed features, for both brain's volumes and thicknesses, reproducing findings from several previous brain's morphometric studies. Finally, we explored how different stratified percentiles evolve with age, finding that aging is not a process that can be described by a mean descriptor but on the contrary should be analyzed by considering different percentile layers with its own specific aging dynamic.

Keywords: Healthy Aging, Voxel-based Morphometry, Surface-based Morphometry

1. INTRODUCTION

Clinical practice in magnetic resonance imaging (MRI) of the brain is a field that uses a well-trained eye to see whether brain structures properties of a patient correspond to a healthy pattern. Analyzed properties usually depend on both the clinical case and the set of MRI sequences used. Anatomical measurements like cortical thickness (CT), grey matter (GM) and white matter (WM) volumes of different structures are an important stage in the clinical inspection, that generally is performed using a by-eye qualitative estimation and not in a quantitative manner and statistically meaningful way.

MRI studies has consistently associated normal aging with loss of neural tissue volume and expansion in cerebrospinal fluid (CSF) cavities such as brain ventricles[1–6] that, as confirmed by postmortem studies, are mainly associated to a reduction of neuropil due to a minor number of dendrites and synapses, and a loss of nerve fibers, and therefore not related to a direct loss of neurons which is relatively limited with age.[7–9]

Over the past 15 years an important number of studies have described changes in brain volumes using different technologies, from manual drawing of regions to semi-automated whole-brain analysis and even fully automated using voxel-based morphometry (VBM) and surface-based morphometry (SBM) analysis finding specific patterns of volume and cortex shrinkage for different regions.[1–5,7] For example Lemaitre and collaborators made one of the firsts studies of aging using SBM where, using 216 healthy volunteers ranging from age 18 to 87 years, they found a greater atrophy rate in frontal and temporal regions than in primary sensitive regions.[7]

Brain morphometry (BM) has also advanced in describing how the brain changes with different pathologies, such as Alzheimer's Disease (AD),[10–13] Parkinson's Disease (PD),[14–17] Schizophrenia (SCZ),[18–21] Hungtington's Disease (HD)[22,23] and Multiple Sclerosis (MS).[24–26] There are numerous examples of brain morphometry

12th International Symposium on Medical Information Processing and Analysis, edited by Eduardo Romero, Natasha Lepore, Jorge Brieva, Ignacio Larrabide, Proc. of SPIE Vol. 10160, 101600B
 · doi: 10.1117/12.2256894

that show its high level of maturity, for example Steenwijk and collaborators published in 2015 a source-based morphometry work in which they suggest that MS is not only a WM but also a GM pathology with distinct and clinically relevant patterns of atrophy.[26] Another evidence of this maturity is the first Food and Drug Administration (FDA)-approved brain morphometry system to be used as clinically significant data (`http://www.cortechslabs.com/neuroquant/general/`).[27–29]
Complementary to these facts, online storage has improved the availability of numerous neuroimaging databases making accessible a growing number of medical data along with their respective brain images.[30–33] These facts altogether open the way for new challenges of combining quantitative imaging-based information with powerful machine learning algorithms to detect anomalies and aiming to optimize medical diagnosis and to make a quantified treatment follow-up. To do this in a successful way a highly rigorous and analytic work is needed because when working in a transdisciplinary field matching biology, statistics, signal processing, mathematics and medicine there is a lot of possibilities to have a bias or fairly undetectable errors.[34]
In this work we used a publicly available database of 600 MR images from healthy subjects to obtain a full normative group of values of various VBM and SBM metrics of the brain at different stages in life using a fully automated processing pipeline with the well-known software package FreeSurfer.[35–48] We also compare the results with previously similar studies and analyze differences in the results.[2,6,7,49]

2. MATERIALS AND METHODS

2.1 Dataset

A publicly available neuroimaging database, IXI Dataset created by Imperial College London (available at `http://brain-development.org/ixi-dataset/`), was used in this work. The database has MRIs of nearly 600 subjects in five different sequences: T1, T2, proton density (PD), magnetic resonance angiography (MRA) and Diffusion-weighted images (DTI) collected at three different hospitals in London: Hammersmith Hospital using a Philips 3T system ($MRIm_1$), Guys Hospital using a Philips 1.5T system ($MRIm_2$) and Institute of Psychiatry using a GE 1.5T system ($MRIm_3$). The subjects enrolled are from different ethnicity, occupation and education level. Because of the goal of this work, only T1 data were used (TR = 9.6 s, TE = 4.6 s, matrix = 208 x 208 and flip angle = 8). Information in the database was filtered to discard samples without complete metadata and duplicated records. The final group of samples includes 538 records composed by 241 males with ages in the range [20.07,86.2] (45.8 +/- 31.8) and 298 females with ages in the range [19.98, 86.32] (49.4 +/- 32.4).

2.2 Data processing

All T1 brain volumes were processed to get a complete morphometrical description for each one. Cortical reconstruction and volumetric segmentation was performed with the FreeSurfer image analysis suite, which is documented and freely available for download at `http://surfer.nmr.mgh.harvard.edu/`. The technical details of these procedures are described in previous studies.[35–48] Briefly, this processing includes removal of non-brain tissue using a hybrid watershed/surface deformation procedure,[46] automated Talairach transformation, segmentation of the subcortical white matter and deep gray matter volumetric structures (including hippocampus, amygdala, caudate, putamen, ventricles)[39,40] intensity normalization,[50] tessellation of the gray matter-white matter boundary, automated topology correction,[38,51] and surface deformation following intensity gradients to optimally place the gray/white and gray/cerebrospinal fluid borders at the location where the greatest shift in intensity defines the transition to the other tissue class.[35–37] Once the cortical models are complete, a number of deformable procedures can be performed for further data processing and analysis including surface inflation,[41] registration to a spherical atlas which is based on individual cortical folding patterns to match cortical geometry across subjects,[42] parcellation of the cerebral cortex into units with respect to gyral and sulcal structure,[43,52] and creation of a variety of surface based data including maps of curvature and sulcal depth. This method uses both intensity and continuity information from the entire three dimensional MR volume in segmentation and deformation procedures to produce representations of cortical thickness, calculated as the closest distance from the gray/white boundary to the gray/CSF boundary at each vertex on the tessellated surface.[37] The maps are created using spatial intensity gradients across tissue classes and are therefore not simply reliant on absolute

signal intensity. The maps produced are not restricted to the voxel resolution of the original data thus are capable of detecting submillimeter differences between groups. Procedures for the measurement of cortical thickness have been validated against histological analysis[53] and manual measurements.[54,55] FreeSurfer morphometric procedures have been demonstrated to show good test-retest reliability across scanner manufacturers and across field strengths.[44,48] At the final the volume, areas and thickness from each segmentation are quantified.
Once the FreeSurfer's process ends, the quantification were post-processed using Python language (2.7v) to transform the data from plan text format (FreeSurfer's output) to a data structure more useful to make a statistical analysis. The final step process express all the volume quantification as a percentage of the estimated intracranial volume (eTIV) (provided also in FreeSurfer's results) to make each measurement comparable between subjects independently of the head size.[56,57]
We used Desikan-Killiany parcellation for cortical areas and thicknesses.[52] These measurements were not normalized.

2.3 Calculation for mean lobe thickness

To compare results with another study performed by Long and collaborators over 314 participants with a similar processing pipeline[6] we calculated a mean cortical thickness for each lobe. To do this we grouped several cortical tags listed in Table 1 and depicted with an example participant's pial surface in Figure 1. We calculated each subject mean lobe thickness as show in Eqs. 1, 2 and 3.

$$Volume_{tag} = thickness_{tag} \times area_{tag} \tag{1}$$

$$Volume_{lobe} = \sum_{i\,in\,tags} Volume_i \tag{2}$$

$$Thickness_{lobe} = \frac{Volume_{lobe}}{\sum_{i\,in\,tags} area_i} \tag{3}$$

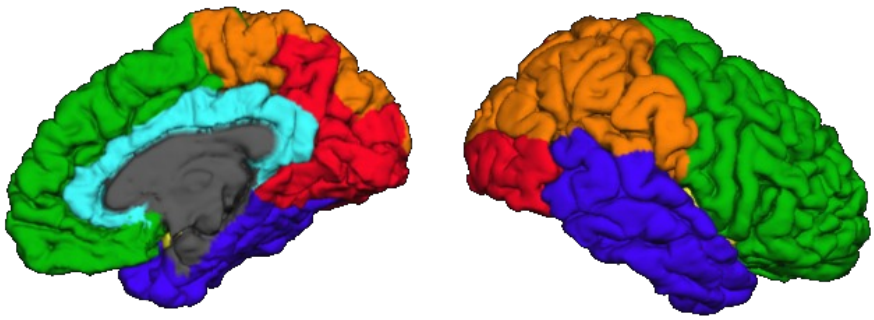

Figure 1. Cortical clustering of regions into lobes: Figure shows in a participant's pial surface the clustering of regions(tags) made to analyze the evolution of mean lobe cortical thickness with aging. Representation colors are: Frontal Lobe in green, Parietal Lobe in orange, Occipital Lobe in red, Temporal Lobe in violet/blue, Cingulate Cortex in magenta and Insula in yellow (it can be seen in between frontal and temporal lobe). It is important to note that the superior portion of the Occipital lobe could not be perfectly delimited because its upper and upper medial zone are part of the big parcel called `superior_parietal` by FreeSurfer's parcellation system.[52]

2.4 Optimization of age clustering

In order to assess the evolution of brain measurements through time, it was needed to split the data into groups according to age ranges. To set these age ranges, two condition were taken into account: (1) the number of participants in each age range have to be between 30 and 90 and (2) the number of participants per group must be as even as possible, considering not only the full group of participants, but also the internal division per

Cerebral Lobe	Tags
Frontal	Frontal Pole, Medial Orbito-Frontal, Lateral Orbito-Frontal, Rostral Middle Frontal, Caudal Middle Frontal, Parsorbitalis, Precentral, Parsopercularis, Parstriangularis, Superior Frontal
Parietal	Post-Central, Para-Central,Supra Marginal, Superior Parietal, Inferior Parietal
Temporal	Superior Temporal, Middle Temporal, Inferior Temporal, Temporal Pole, Transverse Temporal, Entorhinal, Bankssts, Parahippocampal, Fusiform
Insula	Insula
Occipital	Lateral Occipital, Lingual, Cuneus, Precuneus, Pericalcarine
Cingulate	Caudalanterior Cingulate, Rostralanterior Cingulate, Isthmus Cingulate, Posteriorcingulate

Table 1. Region clustering for each lobe mean thickness calculation.[52]

MRI machine ($MRIm_1$, $MRIm_2$ and $MRIm_3$).
To do this we developed an algorithm for the determination of group limits which iterates over possible candidates for number of participant per group (N) and uses a Chi-Square Test for uniform distribution over histograms to optimize age groups distribution (globally and also per MRI machine). Figure 2 shows a schematic flow diagram of the algorithm which consists of the following steps:

1. Subjects' Meta-data (composed by age and MRI machine) is loaded for each study.
2. Subjects are sorted by age in ascending order.
3. Following steps are repeated for N over the range from 30 to 90:
   (a) Subjects are picked one by one in ascending order of age, splitting the data in M groups of N subjects, making the last group (older subjects) to absorb the division residue.
   (b) According to the previous division, the age limits for each group are defined.
   (c) Using these limits (previous step) four histograms are generated. One using all participants and another three using data from each MRI machine.
   (d) For each histogram a Chi-Square Test for uniform distribution is calculated (χ^2), then the mean Chi-Square score ($\bar{\chi^2}$) is computed (see Equation 4) and saved with the age limits.

$$\bar{\chi^2} = mean(\chi^2_{Global}, \chi^2_{MR_1}, \chi^2_{MR_2}, \chi^2_{MR_3}) \tag{4}$$

4. Once iterations finished, the absolute minimum mean Chi-Square score is selected and the optimum age division is obtained (see red circle in Figure 2).

2.5 Assessing healthy aging

The evolution in time of the size of different brain structures (volume or thickness) were assessed by using graphical and statistical tools. Scatter plots were used to study the relationship between brain structure size and subject age. In order to model the evolution for each structure a regression curve was fitted to empirical data and R^2 was taken as goodness of fit. We analyzed the evolution of structures size through successive age ranges in two ways: (1) computing the median and dispersion (box charts and percentiles) for each group and (2) calculating the Percentage Mean Per Year Change Rate ($\%\,CR$) between groups calculated by Equation 5.

$$\%\,CR = \frac{\widetilde{x}_i - \widetilde{x}_{i-1}}{\widetilde{x}_{i-1} \times (\widetilde{t}_i - \widetilde{t}_{i-1})} \times 100 \left[\frac{\%}{year}\right] \tag{5}$$

Where $\widetilde{x}$ is the median value of the structure size in the age group i and $\widetilde{t}$ is the center age on the group intervals. As can be noticed on Eqs. 5 the change rate was expressed as percentage of the previous (younger) group.

3. RESULTS

3.1 Distribution of participants over groups

Age grouping description summarizing all MRI machines and per machine ($MRIm_1$, $MRIm_2$ and $MRIm_3$) is shown in Table 2. As can be seen and it is pointed out later in the discussions, an even distribution of participant per MRI machine could not be achieved because of a mayor unbalance in $MRIm_3$. In any case, a good overall balance was achieved as well as for $MRIm_1$ and $MRIm_2$.

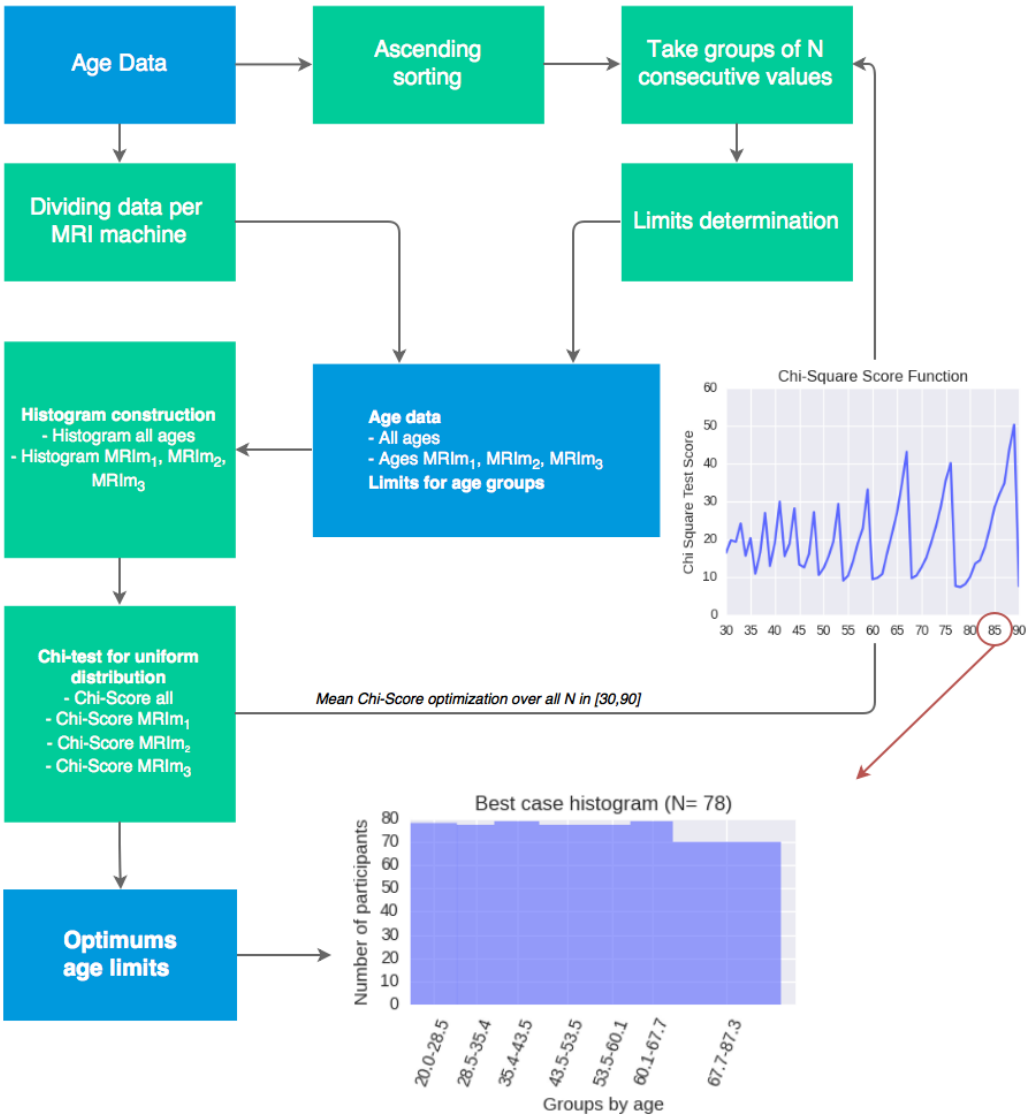

Figure 2. Algorithm for age clustering: schematic flow diagram for optimal age clustering determination. Text-boxes in blue represent data groups while green ones represent functions. The plot at middle right shows the Mean Chi-Square Uniform Test Score obtain while increasing the number of participants in each group from 30 till 90. The histogram at the bottom depicts the optimal distribution obtained by the algorithm.

Age group	Count (Men/Woman)				Mean Age (Range)			
	All	$MRIm_1$	$MRIm_2$	$MRIm_3$	All	$MRIm_1$	$MRIm_2$	$MRIm_3$
20.00 - 28.50	78 (35/43)	36 (19/17)	28 (13/15)	14 (3/11)	24.83 (20.07 - 28.48)	24.71 (20.17 - 28.35)	24.47 (20.07 - 28.12)	25.85 (21.15 - 28.48)
28.50 - 35.40	77 (46/31)	21 (12/9)	40 (25/15)	16 (9/7)	31.66 (28.51 - 35.07)	32.20 (28.56 - 35.02)	31.19 (28.51 - 35.07)	32.10 (28.81 - 34.28)
35.40 - 43.50	79 (39/40)	25 (15/10)	43 (20/23)	11 (4/7)	39.38 (35.41 - 43.46)	39.70 (35.41 - 43.16)	39.51 (35.80 - 43.46)	38.17 (35.46 - 43.08)
43.50 - 53.50	77 (37/40)	22 (12/10)	45 (20/25)	10 (5/5)	48.23 (43.82 - 53.41)	48.78 (43.82 - 53.33)	48.28 (44.02 - 53.41)	46.82 (44.38 - 50.57)
53.50 - 60.10	77 (29/48)	23 (12/11)	52 (17/35)	2 (0/2)	57.25 (53.54 - 60.08)	57.22 (53.57 - 60.07)	57.20 (53.54 - 60.08)	58.89 (58.79 - 58.99)
60.10 - 67.70	79 (25/54)	30 (8/22)	43 (16/27)	6 (1/5)	63.54 (60.10 - 67.53)	63.48 (60.11 - 67.53)	63.48 (60.10 - 67.33)	64.23 (61.37 - 67.24)
67.70 - 87.30	70 (30/40)	23 (9/14)	39 (19/20)	8 (2/6)	72.50 (67.70 - 86.32)	72.13 (67.82 - 81.94)	72.35 (67.70 - 86.20)	74.31 (68.13 - 86.32)

Table 2. Age grouping descriptive information

3.2 Volume changes in healthy aging

To asses global changes a regression analysis was made for main structures and it is shown in Figure 3. Although Total Grey Matter (left side) shows a continuous decay with age, White Matter (center) slightly increases until 50 years old and then it begins to shrink. Meanwhile Ventricular Cavities (right side) seems to follow an exponential expansion over time which can be explained by the overall volume reduction in the surrounding tissue.

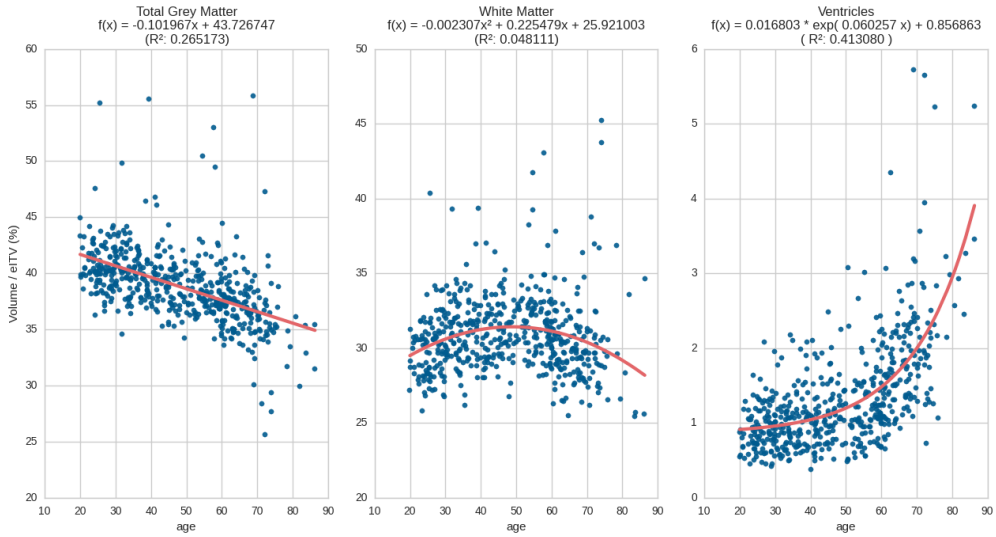

Figure 3. Regression fitting analysis for global changes in the brain: Scatter plot with regression curve for Total Grey Matter (on the left), White Matter (center) an Ventricular cavities (on the right). For each structures the volume was expressed as a percentage of the estimated Total Intracranial Volume (eTIV) through age ranges

For each measurement a regression curve was fitted to empirical data: a linear to Total Grey Matter ($R^2 = 0.26$), a quadratic to White Matter ($R^2 = 0.048$) and a simple exponential to Ventricular Cavities ($R^2 = 0.41$). The low Coefficient of Determination (R^2) for these regression curves is due to the great dispersion because of the intrinsic variability in data despite the normalization.

We obtained evidence of volume reduction in almost all studied subcortical structures. In Figure 4 is shown the normalized volume for different subcortical structures and its change through age ranges only for the left hemisphere given that behavior for the right one is alike.

Although structures like Thalamus, Hippocampus, Amygdala, three portions of the Truncus and Rostrum of the Corpus Callosum (CC) show at young groups a lower rate of reduction than older groups, other structures like Caudate and Pallidum show at young groups a higher rate of reduction than older groups. A continuous volume reduction through all groups can be appreciated in the Putamen, Ventral Diencephalon and Accumbens area, while Splenium of the Corpus Callosum maintain its volume through all ranges.

In Table 3 (upper portion) is shown the Percentage Mean Per Year Change Rate ($\%\,CR$) for the normalized volume for global measurements and all subcortical structures. In the last two periods (56.5-63.5 and 63.5-77)

there is an increase in the absolute values of $\%CR$ which indicates an overall acceleration of the shrinkage of brain structures and also on the enlargement in ventricular cavities as described in previous studies.[1–5,7] In opposition to most subcortical structures, bilateral Caudate nucleus and left Pallidum do not show modifications in the $\%CR$ in elderly participants.

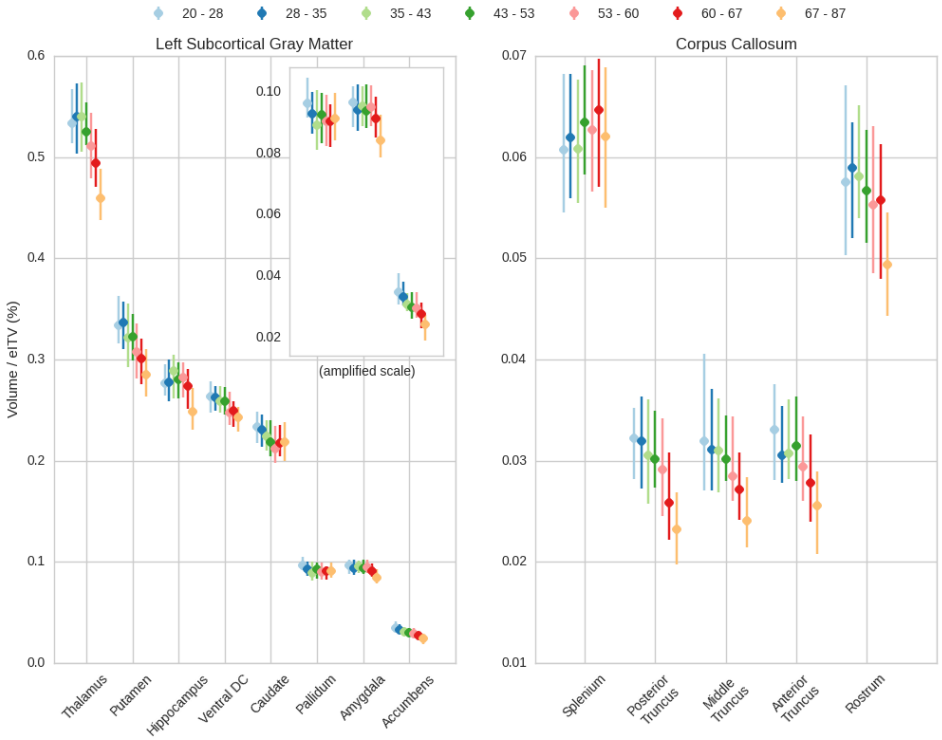

Figure 4. Subcortical structures volume as a percentage of the estimated Total Intracranial Volume (eTIV) through age ranges: On left side, the median value is represented by a dot while the full range from percentiles 25 and 75 is depicted by a bar for Thalamus, Putamen, Hippocampus, Ventral Diencephalon, Caudate, Pallidum, Amygdala and Accumbens area for the left hemisphere (same behavior is observed for the right one). On the upper rectangle an amplified view of Pallidum, Amygdala and Accumbens area is shown. On the right side the same plotting style is shown for all Corpus Callosum portions (Splenium, Posterior, Middle, Anterior Truncus and Rostrum).

3.3 Cortical thickness changes in healthy aging

We obtained cortical thickness measurement for each cortical parcel and for comparison purposes we analyzed the evolution for the each lobe. Results for Frontal cortex are shown in Figure 5, where a constant slope reduction can be appreciated with a similar dispersion over all ages until 70 years old where cases with not linear reduction can be seen. Interestingly, as show in plots for Temporal cortex (Figure 6), Parietal cortex (Figure 7), Insular cortex (Figure 8), Cingulate cortex (Figure 9) and Occipital cortex (in Figure 10), they all exhibit a similar behavior to Frontal cortex (only left lobes are presented because right ones are alike). In the percentile plots on the left side of Figures 5 - 10 it is noticeable that they all have a constant median thickness reduction with age which is evidenced too by the negative slope of the linear regression fitted to the empirical data for each lobe (on the right side).

Although higher boundaries (percentiles 80, 90 and 100) decline at the same pace that the median, lower boundaries (percentiles 0 and 10, not percentile 20) have a more abrupt decline (specially in older groups).

Table 3 (lower portion) shows the Percentage Mean Per Year Change Rate ($\%CR$) with a fairly constant negative rate over aging with an important increase in the last period (63.5 - 77) where shrinking in Frontal, Parietal, Temporal, Occipital and Insular cortices double previous change rates.

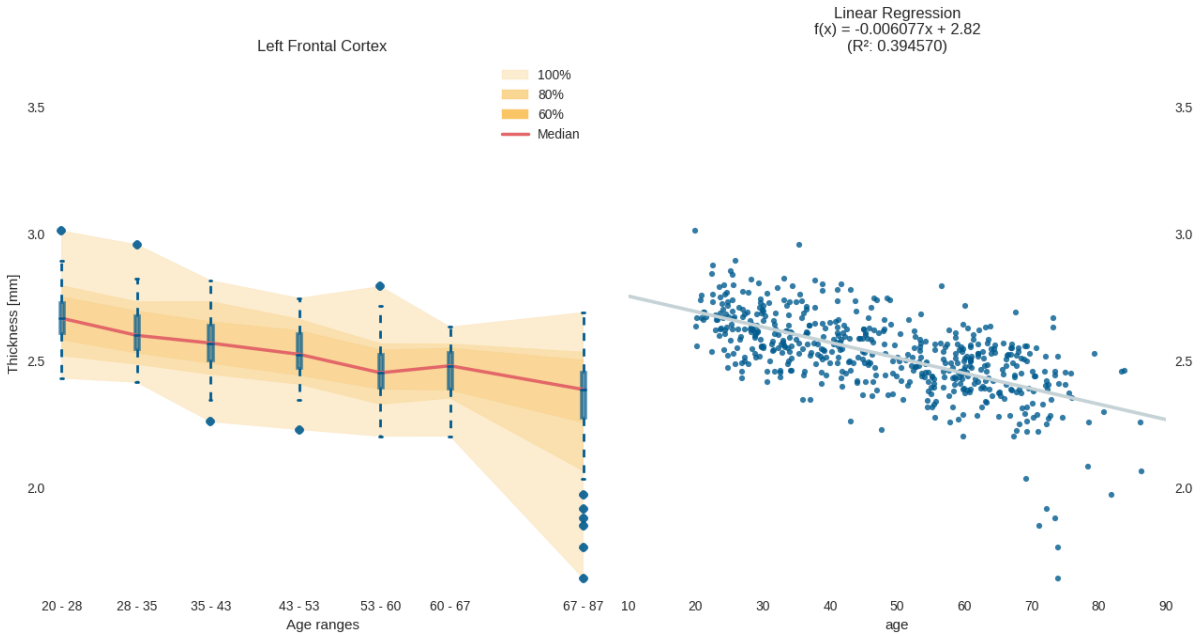

Figure 5. Left Frontal Cortex Thickness through age ranges: On Left side, a percentile plot where medians are bounded by a red line, percentiles 25 and 75 are represented by blue boxes and ninety five percent confident interval with dashed blue lines. Outliers are depicts with blue dots and interval which contain 100%, 80% and 60% of the population are in orange with increasing intensity. On the right side there is a scatter plot of the thickness for each subject age and a linear regression function fitted to the data.

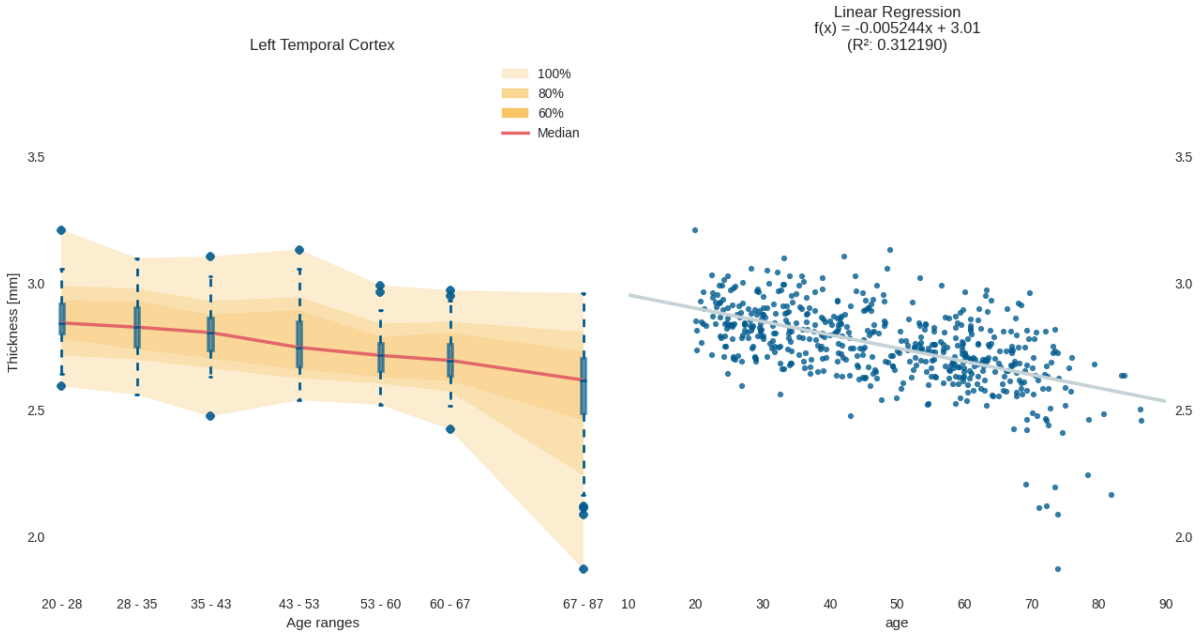

Figure 6. Left Temporal Cortex Thickness through age ranges: On Left side, a percentile plot where medians are bounded by a red line, percentiles 25 and 75 are represented by blue boxes and ninety five percent confident interval with dashed blue lines. Outliers are depicts with blue dots and interval which contain 100%, 80% and 60% of the population are in orange with increasing intensity. On the right side there is a scatter plot of the thickness for each subject age and a linear regression function fitted to the data.

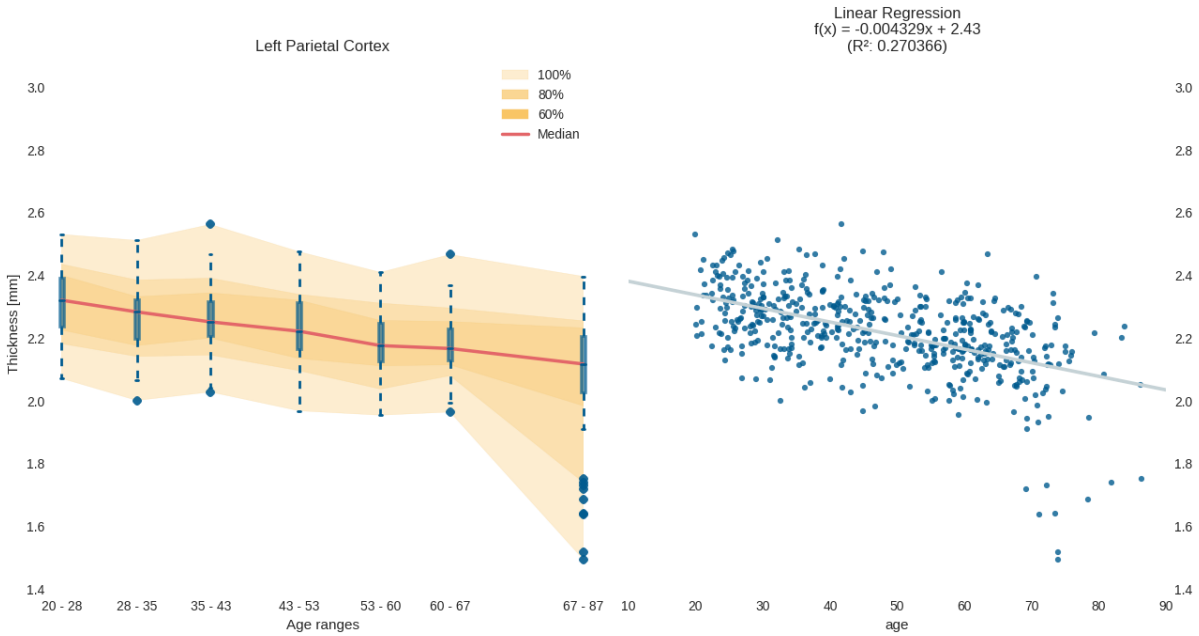

Figure 7. Left Parietal Cortex Thickness through age ranges: On Left side, a percentile plot where medians are bounded by a red line, percentiles 25 and 75 are represented by blue boxes and ninety five percent confident interval with dashed blue lines. Outliers are depicts with blue dots and interval which contain 100%, 80% and 60% of the population are in orange with increasing intensity. On the right side there is a scatter plot of the thickness for each subject age and a linear regression function fitted to the data.

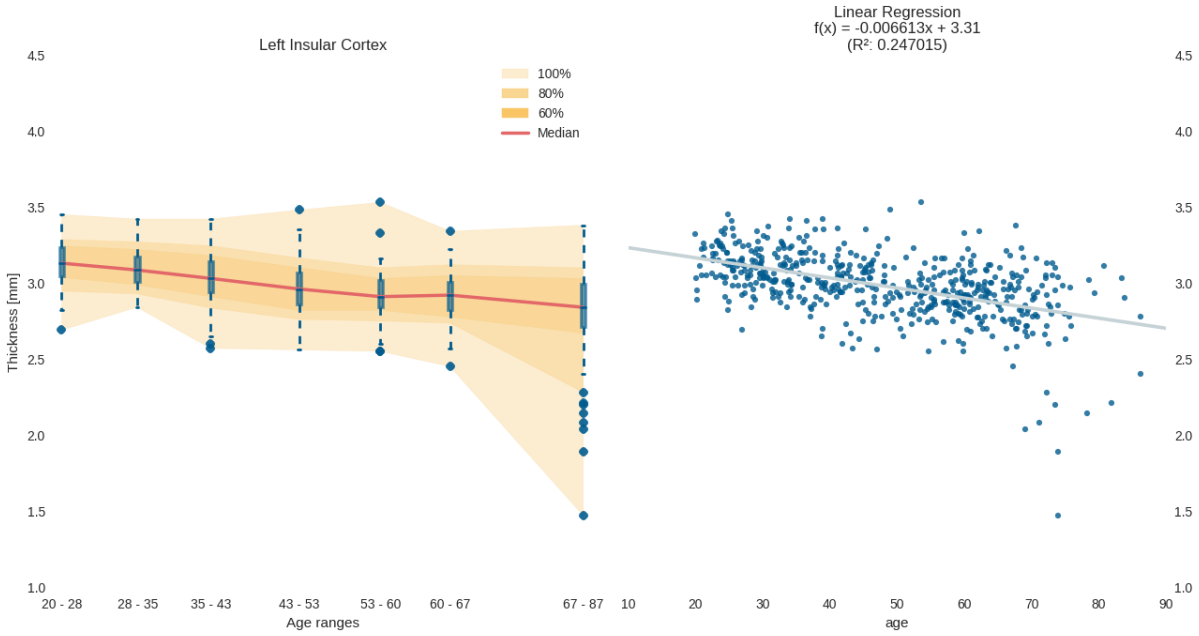

Figure 8. Left Insular Cortex Thickness through age ranges:On Left side, a percentile plot where medians are bounded by a red line, percentiles 25 and 75 are represented by blue boxes and ninety five percent confident interval with dashed blue lines. Outliers are depicts with blue dots and interval which contain 100%, 80% and 60% of the population are in orange with increasing intensity. On the right side there is a scatter plot of the thickness for each subject age and a linear regression function fitted to the data.

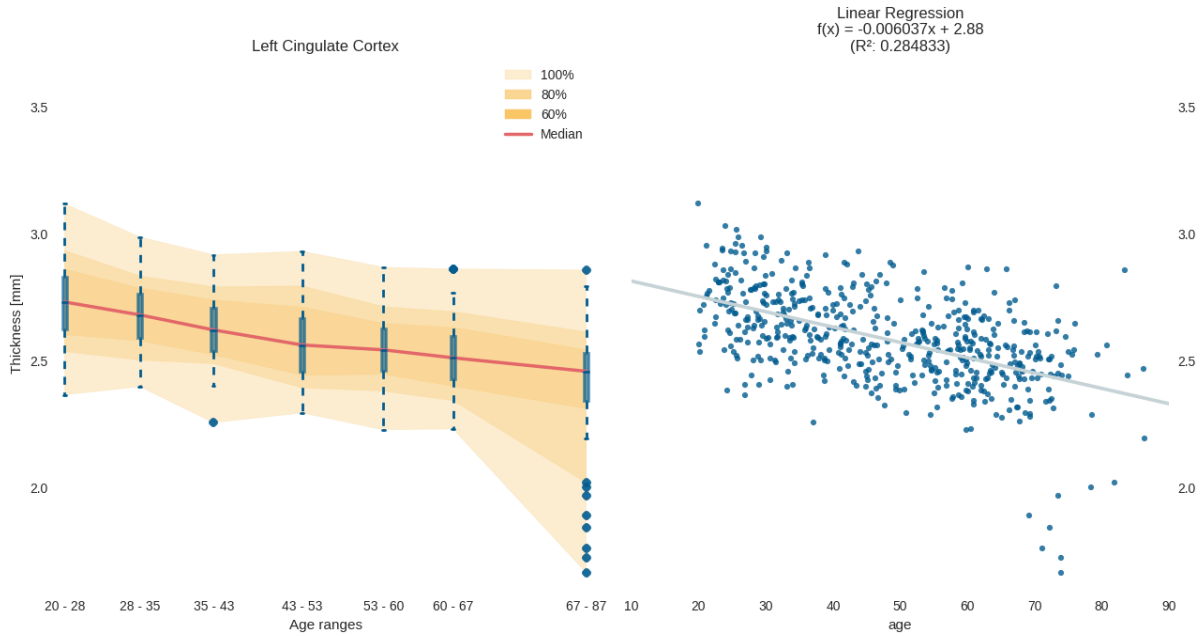

Figure 9. Left Cingulate Cortex Thickness through age ranges: On Left side, a percentile plot where medians are bounded by a red line, percentiles 25 and 75 are represented by blue boxes and ninety five percent confident interval with dashed blue lines. Outliers are depicts with blue dots and interval which contain 100%, 80% and 60% of the population are in orange with increasing intensity. On the right side there is a scatter plot of the thickness for each subject age and a linear regression function fitted to the data.

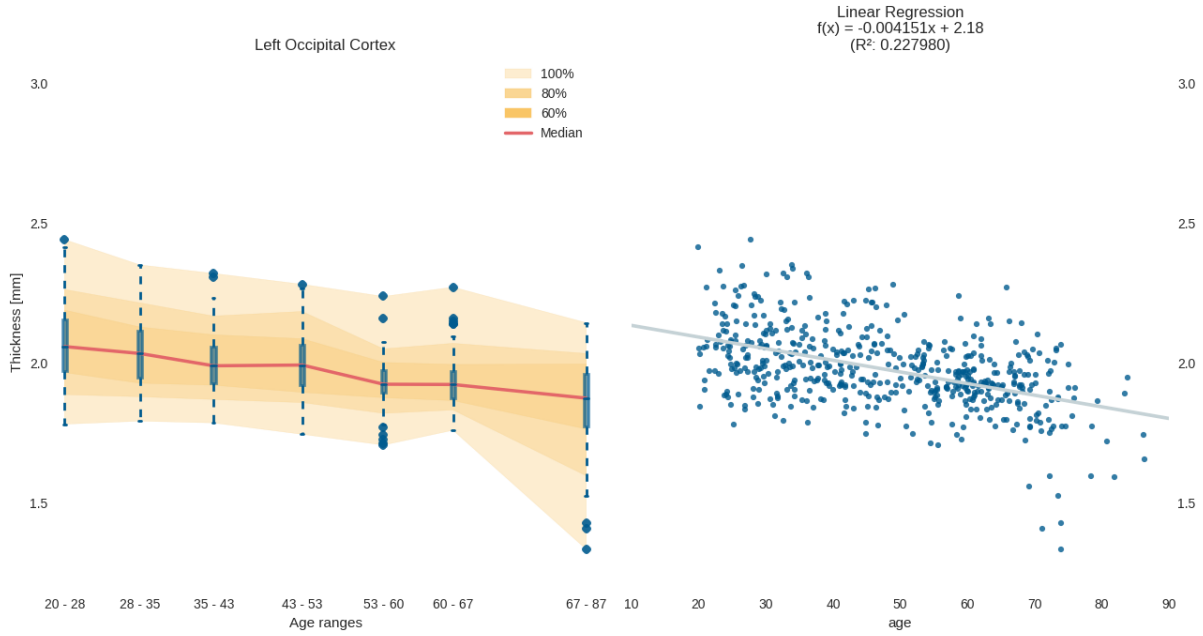

Figure 10. Left Occipital Cortex Thickness through age ranges: On Left side, a percentile plot where medians are bounded by a red line, percentiles 25 and 75 are represented by blue boxes and ninety five percent confident interval with dashed blue lines. Outliers are depicts with blue dots and interval which contain 100%, 80% and 60% of the population are in orange with increasing intensity. On the right side there is a scatter plot of the thickness for each subject age and a linear regression function fitted to the data.

	Age Range	24 - 31.5	31.5 - 39.5	39.5 - 48	48 - 56.5	56.5 - 63.5	63.5 - 77
Normalized Volume	Total Grey Matter	-0.0092	-0.1425	-0.3383***	-0.2786	-0.1680**	-0.3449**
	White Matter	0.2235**	0.2261	0.0606	-0.0288	-0.6303***	-0.0776
	Ventricles	0.5748	1.3543	0.6884	0.7106	5.3984***	2.5732***
	Thalamus (lh)	0.1555	-0.0029	-0.3075	-0.3248*	-0.4665	-0.5111***
	Thalamus (rh)	0.0901	-0.0700	-0.0462	-0.5386**	-0.2589	-0.4161**
	Putamen (lh)	0.0996	-0.5812	0.0215	-0.5479	-0.3261*	-0.3839
	Putamen (rh)	-0.0402	-0.3236	-0.3201**	-0.5411	-0.0990	-0.3038
	Hippocampus (lh)	0.0469	0.5442	-0.3038	0.0605	-0.4037*	-0.6754***
	Hippocampus (rh)	0.1952	0.2216	0.0777	-0.0968	-0.3916**	-0.5610**
	Ventral DC (lh)	-0.0660	-0.1899	0.0002	-0.5210	0.0941	-0.1694
	Ventral DC (rh)	-0.1213	0.0214	-0.0686	-0.2745	-0.1458	-0.2248**
	Caudate (lh)	-0.1580	-0.3865	-0.2794	-0.3589	0.3588	0.0254
	Caudate (rh)	0.1349	-0.0344	-0.3549	-0.0666	0.0729	0.0254
	Pallidum (lh)	-0.4546	-0.5385	0.4327	-0.2723	0.0163	0.0709
	Pallidum (rh)	-0.0295	-0.6272	0.5032	-0.6797	0.1927	-0.4351
	Amygdala (lh)	-0.3129	0.1793	-0.1906	0.1648	-0.5607*	-0.5665**
	Amygdala (rh)	0.2546	0.0146	-0.0813	-0.2144	-0.0596	-0.4666**
	Accumbens (lh)	-0.5394	-0.9460**	-0.4110	-0.1036	-0.9389*	-0.9030***
	Accumbens (rh)	0.1476	-1.1557**	-0.2269	-0.3810	-0.3881	-0.4860**
	CC-Splenium	0.2609	-0.2358	0.4632	-0.1301	0.4365	-0.2975
	CC-Posterior Truncus	-0.1469	-0.5656	-0.1526	-0.3957	-1.6077*	-0.7297**
	CC-Middle Truncus	-0.3597	-0.0256	-0.3173	-0.6651	-0.6442**	-0.8484**
	CC-Anterior Truncus	-1.0016	0.0758	0.2759	-0.7943	-0.7385	-0.5981***
	CC-Rostrum	0.3184	-0.1916	-0.2760	-0.2856	0.1057	-0.8352**
	Cerebellum Cortex (lh)	-0.0784	-0.2677	-0.1545	-0.1610	-0.3609**	-0.2796
	Cerebellum WM (lh)	-0.1449	0.6174	0.2080	-0.1907	-0.4137*	-0.2984
	Cerebellum Cortex (rh)	0.0195	-0.3104	-0.1320	0.0556	-0.9136***	-0.1880
	Cerebellum WM (rh)	-0.2686	0.5525	0.1115	-0.0880	-0.0544	-0.3968
	Brain-Stem	0.1571	0.3638*	0.0822	-0.1842	-0.2392*	-0.2248
Cortical Thickness	Frontal (lh)	-0.3279***	-0.1549	-0.1900*	-0.3464***	0.1579	-0.2762***
	Frontal (rh)	-0.3684***	-0.1025	-0.2381**	-0.2936***	-0.0760	-0.2321***
	Parietal (lh)	-0.2086**	-0.1852	-0.1457*	-0.2482**	-0.0597	-0.1673***
	Parietal (rh)	-0.3019**	0.0063	-0.1525*	-0.3505**	-0.0776	-0.1430***
	Temporal (lh)	-0.0763	-0.0996	-0.2313	-0.1379**	-0.1019	-0.2105***
	Temporal (rh)	-0.2078	-0.0575	-0.2513	-0.1022**	-0.1731*	-0.1916***
	Occipital (lh)	-0.1552	-0.2869	0.0145	-0.4128***	-0.0069	-0.1862***
	Occipital (rh)	-0.0767	-0.2059	-0.0143	-0.4139***	-0.0592	-0.1503**
	Cingulate (lh)	-0.2419*	-0.2934*	-0.2498*	-0.0899	-0.1737	-0.1553**
	Cingulate (rh)	-0.3293***	-0.3609*	-0.1084	-0.1425	-0.1735	-0.1274*
	Insular (lh)	-0.1861	-0.2369*	-0.2544*	-0.2028	0.0482	-0.2008**
	Insular (rh)	0.0000	-0.3268**	-0.2776*	-0.1242	0.0000	-0.2808***

Table 3. Percentage Mean Per Year Change Rate ($\%\,CR$).

*** $p < 0.001$ ** $p < 0.01$ * $p < 0.05$

4. DISCUSSION

This study analyzed the evolution of different cortical and subcortical brain structures through life. Using FreeSurfer, a well-know voxel-based and surface-based morphometry software, and our own Python-based post-processing software we accomplished to measure 135 different brain features in 538 participants from a publicly available database.

As for the comparison of the results with previous studies, in 2001 Good and collaborators published a voxel-based morphometry study over 465 subjects where they describe changes over total grey and white matter and total CSF. The overall results showed a continuous reduction in total grey matter and a two phase evolution for white matter, a first subtle increase until 45 years old and a continuous decrease afterward while CSF showed a seemly exponential expansion.[2] Our results matched all these findings as can be seen in Figure 3.

Another study made by Fjell and collaborators published in 2009 used FreeSurfer to process 883 subjects from 6 different earlier studies in which 1.5T MRI machines from diverse manufacturer were used. A widespread thinning of the brain cortex was found with very similar results to the ones depicted in Figures 5 to 10.[49]

A more recent study published by Long and collaborators in 2012 used a publicly available database of 314 subjects to study healthy aging of the brain finding different results to the ones obtained in this study.[6] A mayor discrepancy was found in ventricles in which the plateau described by Long et. al. in elderly subjects was not observed. Other differences were observed in subcortical volumes but could not been directly compared because of the lack of normalization in Long's work which represents a mayor limitation. As for the analysis in cortical thickness, Long et. al. described a significant thinning for insular cortex that disagree with our findings. It is important to highlight that although Long's research was performed over 314 participant, ages were not evenly distributed with and important bias towards younger ages.

As for the rate of change per year we compared our findings with a research published in 2012 by Lemaitre and collaborators in which they calculated a per year thinning rate for each cortex region that corresponds to our measurements presented in Table 3 (lower portion).[7]

Although our results match with other previously published works, several studies have assessed for the influence of different MRI machines over FreeSurfer's measurements finding subtle (but not clinically relevant) changes in obtained results,[44,48] hence we think that additional work must be made to analyze whether using three different MRI machines (two different manufacturers and two different permanent magnetic fields) could mean any influence in our results. Given the variability observed in the evolution of each measurement with age, we think that it is necessary to adjust a multivariate model to test the influence of the acquisition system over each score, considering into the statistical model the MRI machine and age as explanatory variables and taking into account possible interactions between them. These models have also to be tuned for each particular measurement using a suitable regression model. This issue is going to be afforded in future works.

Another future work is related to Thambisetty and collaborators research published in 2010 in which they found some cortical areas with a sex dependent thickness in elderly population. For that reason we will include variables like sex, academic level and occupation in future works to look for meaningful factors that could modify morphometric measuments.[58]

In conclusion we obtained a quantitative description of brain structural changes in healthy aging. To do this we analyzed structure changes in size over aging in a statistical manner, getting results which represents the intrinsic variability over ageing. The availability of this information allowed us to model brain changes as a dynamical process not only by mean descriptors but also by means of a statistical model, which will be useful to compare pathological samples and also to implement technological optimization in clinical neurosciences.

REFERENCES

[1] Courchesne, E., Chisum, H. J., Townsend, J., Cowles, A., Covington, J., Egaas, B., Harwood, M., Hinds, S., and Press, G. A., "Normal brain development and aging: quantitative analysis at in vivo mr imaging in healthy volunteers 1," *Radiology* **216**(3), 672–682 (2000).

[2] Good, C. D., Johnsrude, I. S., Ashburner, J., Henson, R. N., Fristen, K., and Frackowiak, R. S., "A voxel-based morphometric study of ageing in 465 normal adult human brains," in [*Biomedical Imaging, 2002. 5th IEEE EMBS International Summer School on*], 16–pp, IEEE (2002).

[3] Lemaître, H., Crivello, F., Grassiot, B., Alpérovitch, A., Tzourio, C., and Mazoyer, B., "Age-and sex-related effects on the neuroanatomy of healthy elderly," *Neuroimage* **26**(3), 900–911 (2005).

[4] Smith, C. D., Chebrolu, H., Wekstein, D. R., Schmitt, F. A., and Markesbery, W. R., "Age and gender effects on human brain anatomy: a voxel-based morphometric study in healthy elderly," *Neurobiology of aging* **28**(7), 1075–1087 (2007).
[5] Walhovd, K. B., Fjell, A. M., Reinvang, I., Lundervold, A., Dale, A. M., Eilertsen, D. E., Quinn, B. T., Salat, D., Makris, N., and Fischl, B., "Effects of age on volumes of cortex, white matter and subcortical structures," *Neurobiology of aging* **26**(9), 1261–1270 (2005).
[6] Long, X., Liao, W., Jiang, C., Liang, D., Qiu, B., and Zhang, L., "Healthy aging: an automatic analysis of global and regional morphological alterations of human brain," *Academic radiology* **19**(7), 785–793 (2012).
[7] Lemaitre, H., Goldman, A. L., Sambataro, F., Verchinski, B. A., Meyer-Lindenberg, A., Weinberger, D. R., and Mattay, V. S., "Normal age-related brain morphometric changes: nonuniformity across cortical thickness, surface area and gray matter volume?," *Neurobiology of aging* **33**(3), 617–e1 (2012).
[8] Pakkenberg, B., Pelvig, D., Marner, L., Bundgaard, M. J., Gundersen, H. J. G., Nyengaard, J. R., and Regeur, L., "Aging and the human neocortex," *Experimental gerontology* **38**(1), 95–99 (2003).
[9] Peters, A., "Structural changes in the normally aging cerebral cortex of primates," *Progress in brain research* **136**, 455–465 (2002).
[10] Gutman, B. A., Wang, Y., Yanovsky, I., Hua, X., Toga, A. W., Jack, C. R., Weiner, M. W., Thompson, P. M., Initiative, A. D. N., et al., "Empowering imaging biomarkers of alzheimer's disease," *Neurobiology of aging* **36**, S69–S80 (2015).
[11] Eskildsen, S. F., Coupé, P., Fonov, V. S., Pruessner, J. C., Collins, D. L., Initiative, A. D. N., et al., "Structural imaging biomarkers of alzheimer's disease: predicting disease progression," *Neurobiology of aging* **36**, S23–S31 (2015).
[12] Westman, E., Simmons, A., Muehlboeck, J.-S., Mecocci, P., Vellas, B., Tsolaki, M., Kłoszewska, I., Soininen, H., Weiner, M. W., Lovestone, S., et al., "Addneuromed and adni: similar patterns of alzheimer's atrophy and automated mri classification accuracy in europe and north america," *Neuroimage* **58**(3), 818–828 (2011).
[13] Westman, E., Muehlboeck, J.-S., and Simmons, A., "Combining mri and csf measures for classification of alzheimer's disease and prediction of mild cognitive impairment conversion," *Neuroimage* **62**(1), 229–238 (2012).
[14] Gerrits, N. J., van Loenhoud, A. C., van den Berg, S. F., Berendse, H. W., Foncke, E. M., Klein, M., Stoffers, D., van der Werf, Y. D., and van den Heuvel, O. A., "Cortical thickness, surface area and subcortical volume differentially contribute to cognitive heterogeneity in parkinsons disease," *PloS one* **11**(2), e0148852 (2016).
[15] Burton, E. J., McKeith, I. G., Burn, D. J., Williams, E. D., and OBrien, J. T., "Cerebral atrophy in parkinsons disease with and without dementia: a comparison with alzheimers disease, dementia with lewy bodies and controls," *Brain* **127**(4), 791–800 (2004).
[16] Beyer, M. K., Janvin, C. C., Larsen, J. P., and Aarsland, D., "A magnetic resonance imaging study of patients with parkinsons disease with mild cognitive impairment and dementia using voxel-based morphometry," *Journal of Neurology, Neurosurgery & Psychiatry* **78**(3), 254–259 (2007).
[17] Jubault, T., Gagnon, J.-F., Karama, S., Ptito, A., Lafontaine, A.-L., Evans, A. C., and Monchi, O., "Patterns of cortical thickness and surface area in early parkinson's disease," *Neuroimage* **55**(2), 462–467 (2011).
[18] Mamah, D., Alpert, K. I., Barch, D. M., Csernansky, J. G., and Wang, L., "Subcortical neuromorphometry in schizophrenia spectrum and bipolar disorders," *NeuroImage: Clinical* **11**, 276–286 (2016).
[19] Shenton, M. E., Dickey, C. C., Frumin, M., and McCarley, R. W., "A review of mri findings in schizophrenia," *Schizophrenia research* **49**(1), 1–52 (2001).
[20] Xu, L., Groth, K. M., Pearlson, G., Schretlen, D. J., and Calhoun, V. D., "Source-based morphometry: The use of independent component analysis to identify gray matter differences with application to schizophrenia," *Human brain mapping* **30**(3), 711–724 (2009).
[21] Schnack, H. G., Nieuwenhuis, M., van Haren, N. E., Abramovic, L., Scheewe, T. W., Brouwer, R. M., Pol, H. E. H., and Kahn, R. S., "Can structural mri aid in clinical classification? a machine learning study in two independent samples of patients with schizophrenia, bipolar disorder and healthy subjects," *Neuroimage* **84**, 299–306 (2014).

[22] Younes, L., Ratnanather, J. T., Brown, T., Aylward, E., Nopoulos, P., Johnson, H., Magnotta, V. A., Paulsen, J. S., Margolis, R. L., Albin, R. L., et al., "Regionally selective atrophy of subcortical structures in prodromal hd as revealed by statistical shape analysis," *Human brain mapping* **35**(3), 792–809 (2014).

[23] Kassubek, J., Gaus, W., and Landwehrmeyer, G. B., "Evidence for more widespread cerebral pathology in early hd: an mri-based morphometric analysis," *Neurology* **62**(3), 523–524 (2004).

[24] Bendfeldt, K., Kuster, P., Traud, S., Egger, H., Winklhofer, S., Mueller-Lenke, N., Naegelin, Y., Gass, A., Kappos, L., Matthews, P. M., et al., "Association of regional gray matter volume loss and progression of white matter lesions in multiple sclerosisa longitudinal voxel-based morphometry study," *Neuroimage* **45**(1), 60–67 (2009).

[25] Prinster, A., Quarantelli, M., Orefice, G., Lanzillo, R., Brunetti, A., Mollica, C., Salvatore, E., Morra, V. B., Coppola, G., Vacca, G., et al., "Grey matter loss in relapsing–remitting multiple sclerosis: a voxel-based morphometry study," *Neuroimage* **29**(3), 859–867 (2006).

[26] Steenwijk, M. D., Geurts, J. J., Daams, M., Tijms, B. M., Wink, A. M., Balk, L. J., Tewarie, P. K., Uitdehaag, B. M., Barkhof, F., Vrenken, H., et al., "Cortical atrophy patterns in multiple sclerosis are non-random and clinically relevant," *Brain* , awv337 (2015).

[27] Brewer, J., "Fully-automated volumetric mri with normative ranges: translation to clinical practice," *Behavioural neurology* **21**(1-2), 21–28 (2009).

[28] Ross, D. E., Ochs, A. L., Seabaugh, J., and Henshaw, T., "Neuroquant® revealed hippocampal atrophy in a patient with traumatic brain injury," *The Journal of neuropsychiatry and clinical neurosciences* **24**(1), E33–E33 (2012).

[29] Ross, D. E., Ochs, A. L., Seabaugh, J. M., and Shrader, C. R., "Man versus machine: Comparison of radiologists interpretations and neuroquant® volumetric analyses of brain mris in patients with traumatic brain injury," *The Journal of neuropsychiatry and clinical neurosciences* **25**(1), 32–39 (2013).

[30] Wyman, B. T., Harvey, D. J., Crawford, K., Bernstein, M. A., Carmichael, O., Cole, P. E., Crane, P. K., DeCarli, C., Fox, N. C., Gunter, J. L., et al., "Standardization of analysis sets for reporting results from adni mri data," *Alzheimer's & Dementia* **9**(3), 332–337 (2013).

[31] Simmons, A., Westman, E., Muehlboeck, S., Mecocci, P., Vellas, B., Tsolaki, M., Kłoszewska, I., Wahlund, L.-O., Soininen, H., Lovestone, S., et al., "The addneuromed framework for multi-centre mri assessment of alzheimer's disease: experience from the first 24 months," *International journal of geriatric psychiatry* **26**(1), 75–82 (2011).

[32] Hodge, M. R., Horton, W., Brown, T., Herrick, R., Olsen, T., Hileman, M. E., McKay, M., Archie, K. A., Cler, E., Harms, M. P., et al., "Connectomedbsharing human brain connectivity data," *Neuroimage* **124**, 1102–1107 (2016).

[33] Marcus, D. S., Wang, T. H., Parker, J., Csernansky, J. G., Morris, J. C., and Buckner, R. L., "Open access series of imaging studies (oasis): cross-sectional mri data in young, middle aged, nondemented, and demented older adults," *Journal of cognitive neuroscience* **19**(9), 1498–1507 (2007).

[34] Eklund, A., Nichols, T. E., and Knutsson, H., "Cluster failure: Why fmri inferences for spatial extent have inflated false-positive rates," *Proceedings of the National Academy of Sciences* , 201602413 (2016).

[35] Dale, A. M., Fischl, B., and Sereno, M. I., "Cortical surface-based analysis: I. segmentation and surface reconstruction," *Neuroimage* **9**(2), 179–194 (1999).

[36] Dale, A. M. and Sereno, M. I., "Improved localizadon of cortical activity by combining eeg and meg with mri cortical surface reconstruction: a linear approach," *Journal of cognitive neuroscience* **5**(2), 162–176 (1993).

[37] Fischl, B. and Dale, A. M., "Measuring the thickness of the human cerebral cortex from magnetic resonance images," *Proceedings of the National Academy of Sciences* **97**(20), 11050–11055 (2000).

[38] Fischl, B., Liu, A., and Dale, A. M., "Automated manifold surgery: constructing geometrically accurate and topologically correct models of the human cerebral cortex," *IEEE transactions on medical imaging* **20**(1), 70–80 (2001).

[39] Fischl, B., Salat, D. H., Busa, E., Albert, M., Dieterich, M., Haselgrove, C., Van Der Kouwe, A., Killiany, R., Kennedy, D., Klaveness, S., et al., "Whole brain segmentation: automated labeling of neuroanatomical structures in the human brain," *Neuron* **33**(3), 341–355 (2002).

[40] Fischl, B., Salat, D. H., van der Kouwe, A. J., Makris, N., Ségonne, F., Quinn, B. T., and Dale, A. M., "Sequence-independent segmentation of magnetic resonance images," *Neuroimage* **23**, S69–S84 (2004).

[41] Fischl, B., Sereno, M. I., and Dale, A. M., "Cortical surface-based analysis: Ii: inflation, flattening, and a surface-based coordinate system," *Neuroimage* **9**(2), 195–207 (1999).

[42] Fischl, B., Sereno, M. I., Tootell, R. B., Dale, A. M., et al., "High-resolution intersubject averaging and a coordinate system for the cortical surface," *Human brain mapping* **8**(4), 272–284 (1999).

[43] Fischl, B., van der Kouwe, A., Destrieux, C., Halgren, E., Ségonne, F., Salat, D. H., Busa, E., Seidman, L. J., Goldstein, J., Kennedy, D., et al., "Automatically parcellating the human cerebral cortex," *Cerebral cortex* **14**(1), 11–22 (2004).

[44] Han, X., Jovicich, J., Salat, D., van der Kouwe, A., Quinn, B., Czanner, S., Busa, E., Pacheco, J., Albert, M., Killiany, R., et al., "Reliability of mri-derived measurements of human cerebral cortical thickness: the effects of field strength, scanner upgrade and manufacturer," *Neuroimage* **32**(1), 180–194 (2006).

[45] Jovicich, J., Czanner, S., Greve, D., Haley, E., van der Kouwe, A., Gollub, R., Kennedy, D., Schmitt, F., Brown, G., MacFall, J., et al., "Reliability in multi-site structural mri studies: effects of gradient non-linearity correction on phantom and human data," *Neuroimage* **30**(2), 436–443 (2006).

[46] Ségonne, F., Dale, A., Busa, E., Glessner, M., Salat, D., Hahn, H., and Fischl, B., "A hybrid approach to the skull stripping problem in mri," *Neuroimage* **22**(3), 1060–1075 (2004).

[47] Reuter, M., Rosas, H. D., and Fischl, B., "Highly accurate inverse consistent registration: a robust approach," *Neuroimage* **53**(4), 1181–1196 (2010).

[48] Reuter, M., Schmansky, N. J., Rosas, H. D., and Fischl, B., "Within-subject template estimation for unbiased longitudinal image analysis," *Neuroimage* **61**(4), 1402–1418 (2012).

[49] Fjell, A. M., Westlye, L. T., Amlien, I., Espeseth, T., Reinvang, I., Raz, N., Agartz, I., Salat, D. H., Greve, D. N., Fischl, B., et al., "High consistency of regional cortical thinning in aging across multiple samples," *Cerebral cortex* , bhn232 (2009).

[50] Sled, J. G., Zijdenbos, A. P., and Evans, A. C., "A nonparametric method for automatic correction of intensity nonuniformity in mri data," *IEEE transactions on medical imaging* **17**(1), 87–97 (1998).

[51] Ségonne, F., Pacheco, J., and Fischl, B., "Geometrically accurate topology-correction of cortical surfaces using nonseparating loops," *IEEE transactions on medical imaging* **26**(4), 518–529 (2007).

[52] Desikan, R. S., Ségonne, F., Fischl, B., Quinn, B. T., Dickerson, B. C., Blacker, D., Buckner, R. L., Dale, A. M., Maguire, R. P., Hyman, B. T., et al., "An automated labeling system for subdividing the human cerebral cortex on mri scans into gyral based regions of interest," *Neuroimage* **31**(3), 968–980 (2006).

[53] Rosas, H., Liu, A., Hersch, S., Glessner, M., Ferrante, R., Salat, D., van Der Kouwe, A., Jenkins, B., Dale, A., and Fischl, B., "Regional and progressive thinning of the cortical ribbon in huntingtons disease," *Neurology* **58**(5), 695–701 (2002).

[54] Kuperberg, G. R., Broome, M. R., McGuire, P. K., David, A. S., Eddy, M., Ozawa, F., Goff, D., West, W. C., Williams, S. C., van der Kouwe, A. J., et al., "Regionally localized thinning of the cerebral cortex in schizophrenia," *Archives of general psychiatry* **60**(9), 878–888 (2003).

[55] Salat, D. H., Buckner, R. L., Snyder, A. Z., Greve, D. N., Desikan, R. S., Busa, E., Morris, J. C., Dale, A. M., and Fischl, B., "Thinning of the cerebral cortex in aging," *Cerebral cortex* **14**(7), 721–730 (2004).

[56] Whitwell, J. L., Crum, W. R., Watt, H. C., and Fox, N. C., "Normalization of cerebral volumes by use of intracranial volume: implications for longitudinal quantitative mr imaging," *American Journal of Neuroradiology* **22**(8), 1483–1489 (2001).

[57] Buckner, R. L., Head, D., Parker, J., Fotenos, A. F., Marcus, D., Morris, J. C., and Snyder, A. Z., "A unified approach for morphometric and functional data analysis in young, old, and demented adults using automated atlas-based head size normalization: reliability and validation against manual measurement of total intracranial volume," *Neuroimage* **23**(2), 724–738 (2004).

[58] Thambisetty, M., Wan, J., Carass, A., An, Y., Prince, J. L., and Resnick, S. M., "Longitudinal changes in cortical thickness associated with normal aging," *Neuroimage* **52**(4), 1215–1223 (2010).